Variable Contributions of Tyrosine Residues to the Structural and Spectroscopic Properties of the Factor for Inversion Stimulation†

Sarah Boswell,‡ John Mathew,‡ Michael Beach,§ Robert Osuna,|| and Wilfredo Colón*,‡

Department of Chemistry and Chemical Biology, Rensselaer Polytechnic Institute, 110 Eighth Street, Troy, New York 12180, Department of Biological Sciences, State University of New York at Albany, Albany, New York 12222, and Physics, Chemistry, and Biological Sciences, Southern Polytechnic State University, 1100 South Marietta Parkway, Marietta, Georgia 30060

Received August 12, 2003; Revised Manuscript Received January 13, 2004

ABSTRACT: The diverse roles of tyrosine residues in proteins may be attributed to their dual hydrophobic and polar nature, which can result in hydrophobic and ring stacking interactions, as well as hydrogen bonding. The small homodimeric DNA binding protein, factor for inversion stimulation (FIS), contains four tyrosine residues located at positions 38, 51, 69, and 95, each involved in specific intra- or intermolecular interactions. To investigate their contributions to the stability, flexibility, and spectroscopic properties of FIS, each one was independently mutated to phenylalanine. Equilibrium denaturation experiments show that Tyr95 and Tyr51 stabilize FIS by about 2 and 1 kcal/mol, respectively, as a result of their involvement in a hydrogen bond−salt bridge network. In contrast, Tyr38 destabilizes FIS by about 1 kcal/mol due to the placement of a hydroxyl group in a hydrophobic environment. The stability of FIS was not altered when the solvent-exposed Tyr69 was mutated. Limited proteolysis with trypsin and V8 proteases was used to monitor the flexibility of the C-terminus (residues 71−98) and the dimer core (residues 26−70), respectively. The results for Y95F and Y51F FIS revealed a different proteolytic susceptibility of the dimer core compared to the C-terminus, suggesting an increased flexibility of the latter. DNA binding affinity of the various FIS mutants was only modestly affected and correlated inversely with the C-terminal flexibility probed by trypsin proteolysis. Deconvolution of the fluorescence contribution of each mutant revealed that it varies in intensity and direction for each tyrosine in WT FIS, highlighting the role of specific interactions and the local environment in determining the fluorescence of tyrosine residues. The significant changes in stability, flexibility, and signals observed for the Y51F and Y95F mutations are attributed to their coupled participation in the hydrogen bond−salt bridge network. These results highlight the importance of tyrosine hydrogen-bonding and packing interactions for the stability of FIS and demonstrate the varying roles that tyrosine residues can play on the structural and spectroscopic properties of even small proteins.

Research conducted over the past decade has underscored the importance of hydrogen bonding to protein stability (*1*−*6*). The mutation of a tyrosine residue for phenylalanine is one of the most conservative mutations that can be made in a protein to probe the role of hydrogen bonding in protein stability. Thus, tyrosine residues of several proteins have been mutated to phenylalanine to investigate the importance of hydrogen bonding to protein stability (*3*, *7*−*10*), as well as for studying other roles of tyrosine residues, such as their biological function (*9*, *11*−*17*), dimerization (*18*, *19*), and contribution to spectroscopic signals (*20*−*25*). While the role of tyrosine hydrogen bonding in maintaining the proper conformation for binding various ligands has been studied (*14*−*16*, *26*), its more general impact on the local dynamics of the native state and its corresponding functional consequence have received less attention. Of all the properties of tyrosine residues, their contributions to spectroscopic signals have been investigated the least, especially when compared to the data available for tryptophan residues (*27*−*35*). Furthermore, there is no comprehensive study that investigates the contribution of tyrosine residues to the function, stability, dynamics, and spectroscopic signals of a protein. In this work we have used the protein factor for inversion stimulation (FIS)[1] to gain a global understanding of how its four tyrosine residues contribute to the various properties of this protein.

FIS is a 22.4 kDa homodimeric DNA binding protein found in *Escherichia coli* and other enteric bacteria (*36*−

† This work was supported by grants from the National Science Foundation (NSF MCB-9984913 to W.C.) and National Institutes of Health (NIH GM52051 to R.O.). J.M. was partially supported by a Howard Hughes Medical Institute undergraduate research program. S.B. is a NSF Graduate Fellow.

* Address correspondence to this author. Fax: (518) 276-4887. E-mail: colonw@rpi.edu.

‡ Rensselaer Polytechnic Institute.

§ Southern Polytechnic State University.

|| State University of New York at Albany.

[1] Abbreviations: bp, base pair; CD, circular dichroism; C_m, transition midpoint; far-UV, far-ultraviolet; FIS, factor for inversion stimulation; MALDI, matrix-assisted laser desorption ionization; MS, mass spectrometry; MW, molecular weight; near-UV, near-ultraviolet; PB, potassium phosphate buffer; SDS−PAGE, sodium dodecyl sulfate−polyacrylamide gel electrophoresis; Tris-HCl, tris(hydroxymethyl)-aminomethane hydrochloride; WT, wild type; Y → F, collective mutations in which tyrosine was changed to phenylalanine.

10.1021/bi035441k CCC: $27.50
Published on Web 02/17/2004

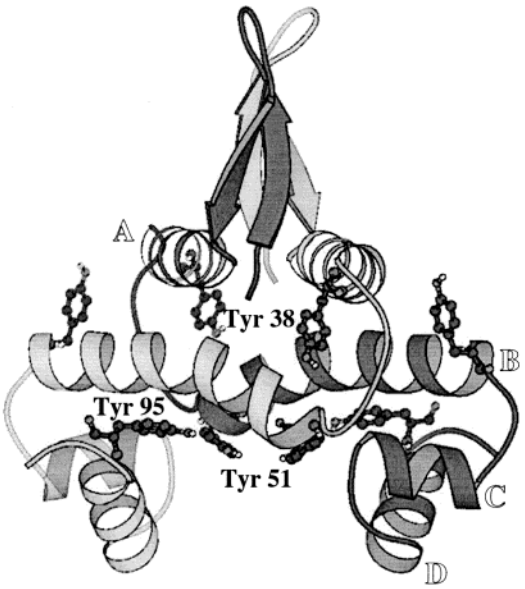

FIGURE 1: Ribbon diagram of the 3D structure of FIS (*42*, *43*, *47*, *49*) with the tyrosine residues highlighted. The four α-helices are labeled A through D. The figure was prepared using the program MOLSCRIPT (*89*).

38) and is involved in various functions, including the stimulation of site-specific DNA inversion reactions catalyzed by the Hin and Gin family of recombinases (*39*−*41*). It has four tyrosine residues scattered throughout the protein, at positions 95, 69, 51, and 38 (Figure 1), and no tryptophan residues. A blast search of the available genomic database reveals that over 30 bacterial species contain a *fis* gene, and their deduced amino acid sequences indicate that these four tyrosines are highly conserved (Figure 2), suggesting that they may have important functional or structural roles. An examination of the crystal structure (*42*, *43*) of *E. coli* FIS reveals that the tyrosines are involved in both intra- and intermolecular interactions. Tyr38 is in the A-helix on the N-terminus of FIS (Figure 1) and is conserved with 97% sequence identity among known FIS sequences (Figure 2). Only 25% of Tyr38 is solvent exposed in the crystal structure, and its hydroxyl group is buried inside a hydrophobic pocket of the protein with no hydrogen-bonding partner (Figure 3A). Tyr51, which is 20% solvent exposed, is located at the beginning of the B-helix, close in three-dimensional space to the C-terminus of FIS (Figure 1). Tyr51 makes complex intermolecular hydrogen-bonding interactions with charged side chains in the B- and D-helices of the opposite subunit (Figure 3B). The importance of this interaction seems to be reflected in the 100% identity conservation of Tyr51 among the various known FIS protein sequences (Figure 2). Tyr69 is located on the B-helix at the opposite end of Tyr51 (Figure 1) and is involved in an intermolecular ring stacking interaction with Phe39 (Figure 3C). It is the most solvent-exposed (50%) tyrosine in FIS and makes no hydrogen bonds to other residues. Tyr69 has the lowest sequence conservation of the tyrosine residues in FIS, at only 66% sequence identity (Figure 2). However, this residue is a histidine in 23% of the sequences (Figure 2), which should be able to replace Tyr69 in the ring stacking interaction. Tyr95 is mostly buried with only 10% of the side chain exposed to solvent. It is located at the C-terminus of FIS in helix D (Figure 1), which is a highly charged region of the protein. Tyr95 shows 86% identity conservation (Figure 2) and is involved in hydrogen bonding with charged residues (Figure 3D). Tyr95 differs from Tyr51 in that it is involved in intramolecular interactions within the D-helix and across to the B-helix of the same subunit (Figure 3).

The differences in the local environments surrounding the tyrosine residues in FIS suggest that their contributions to protein stability, local dynamics, spectroscopic properties, and function may be different from each other. Therefore, FIS may be a good model system for a comprehensive study to determine the contribution of tyrosine hydrogen bonding to these properties. To investigate the roles of the environment and hydrogen-bonding potential of each of the tyrosine residues, four independent phenylalanine substitutions have been performed, creating the mutants Y95F, Y69F, Y51F, and Y38F (collectively, the Y → F FIS mutants). DNA binding assays, equilibrium denaturations, limited proteolysis, and fluorescence and near-UV CD spectral analysis were performed on the four Y → F FIS mutants. The results emphasize the utility of tyrosine fluorescence for monitoring protein folding and add insight into our understanding of the interplay between the local environment of tyrosines and the resulting effect on the spectroscopic signal, function, flexibility, and stability of even small proteins like FIS.

MATERIALS AND METHODS

Generation, Expression, and Purification of FIS Mutants. The Y → F FIS mutations were made as previously described (*44*). In the first PCR reaction for Y38F and Y51F FIS, the primers 5′-TGAGCAAAA**A**AGTTCTTCAG-3′ and 5′-ACCAGCTCA**A**AGAGGTCATTC-3′ were used, respectively (mutations shown in bold, codon region underlined), together with plasmid pLF330 and a second primer, oRO320 (5′-GGAATTCCATATGTTCGAACAACGCG-3′), that anneals to a sequence at the beginning of *fis* and creates an *Nde*I and an *Eco*RI recognition sequence. Plasmid pLF330 contains the wild-type (WT) *fis* gene inserted within the *Nde*I and *Bam*HI restriction sites of the expression vector pET11c (New England BioLabs). The resulting PCR products were separated by electrophoresis on a 5% polyacrylamide gel, purified by the crush and soak method (*45*), and used as a megaprimer for a second PCR with pLF330 as template and the primer oRO319 (5′-CGGGATCCAAGCATTTAGCTAACC-3′) that anneals to a sequence downstream of the termination codon of *fis* and creates a *Bam*HI recognition sequence. In the first PCR for Y69F FIS, an upstream primer, 5′-GGTGATGCAAT**T**CACCCGTGGTAAC-3′, was used together with the primer oRO319 and pLF330 as template. The product of this PCR was separated by electrophoresis and used as a megaprimer for a second PCR together with the upstream primer oRO320. In creating the Y95F FIS mutant, only one PCR reaction was required, using oRO320 and a primer at the end of the *fis* gene (5′-CGGGATCCTTAGTTCATGCCG**A**ATTTTTTCAATTTTTTACAGCAGCG-3′) containing the sequence of the termination codon of *fis*, a *Bam*HI recognition sequence, and a mutation specifying the change of the Tyr95 codon to a phenylalanine. The resulting DNA fragments carrying the entire *fis* gene with each Y → F mutation were purified by gel electrophoresis, cleaved with *Nde*I and *Bam*HI, and ligated into the *Nde*I and *Bam*HI sites of pET11c. The resulting plasmids were transformed into *E. coli* strain RO845 (*ara* Δ[*lac- pro*]

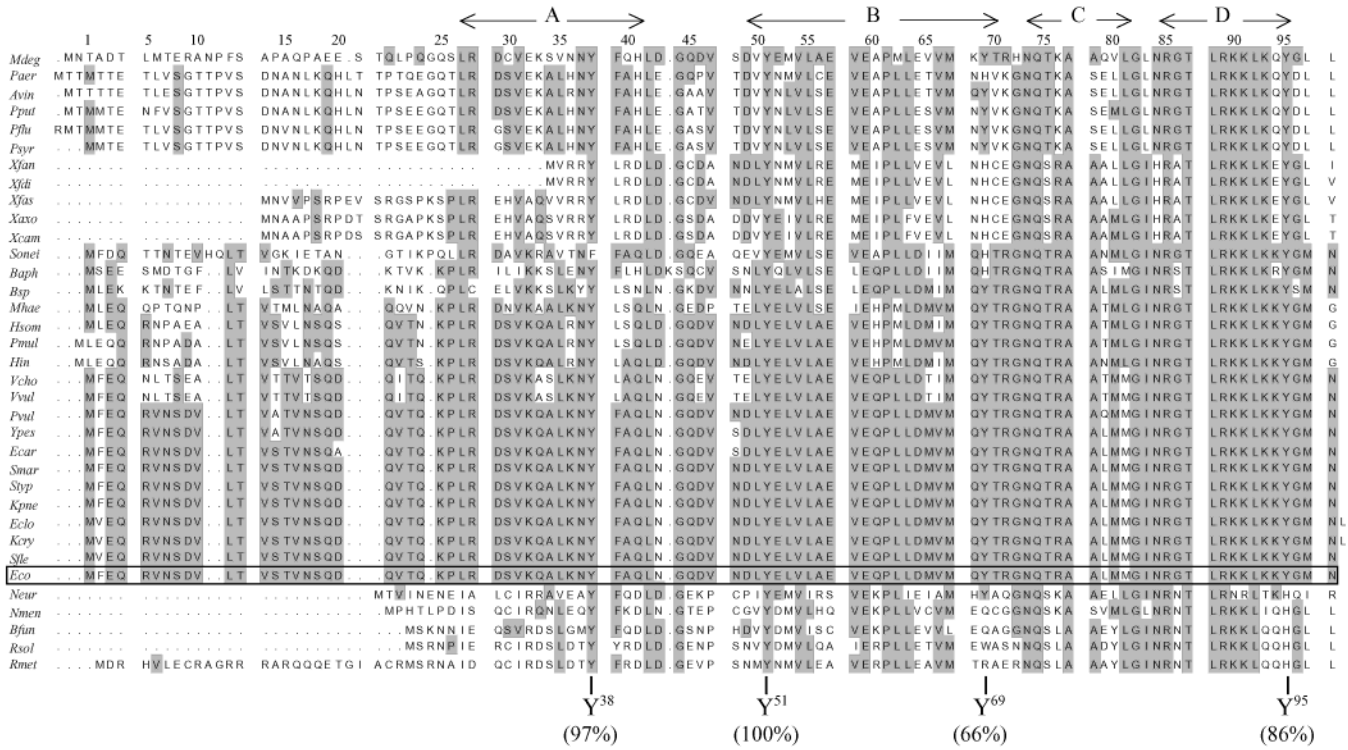

FIGURE 2: Comparison of bacterial FIS sequences identified in a Blast search (*52*) aligned using MultAlin (*53*). The shaded residues designate the identity conservation at each position. Dots represent gaps to bring the sequences into alignment. The numbers at the top indicate the position of residues according to those of *E. coli* FIS, and the labeled arrows indicate the regions containing α-helices. The position of the four tyrosine residues and their percent identity among the FIS sequences are indicated underneath. The bacterial abbreviations in order of appearance from top to bottom: *Mdeg*, *Microbulbifer degradans*; *Paer*, *Pseudomonas aeruginosa*; *Avin*, *Azobacter vinelandii*; *Pput*, *Pseudomonas putida*; *Pflu*, *Pseudomonas fluorescens*; *Psyr*, *Pseudomonas syringae*; *Xfan*, *Xylella fastidiosa* Ann-1; *Xfdi*, *Xylella fastidiosa* Dixon; *Xfas*, *Xylella fastidiosa*; *Xaxo*, *Xanthomonas axonopodis*; *Xcam*, *Xanthomonas campestris*; *Sonei*, *Shewanella oneidensis*; *Baph*, *Buchnera aphidocola*; *Bsp*, *Buchnera* sp. APS; *Mhae*, *Mannheimia haemolytica*; *Hsom*, *Haemophilus somnus*; *Pmul*, *Pasteruella multocida*; *Hin*, *Haemophlus influenzae*; *Vcho*, *Vibrio cholerae*; *Vvul*, *Vibrio vulnificus*; *Pvul*, *Proteus vulgaris*; *Ypes*, *Yersinia pestis*; *Ecar*, *Erwinia carotovora*; *Smar*, *Serratia marcescens*; *Styp*, *Salmonella typhimurium*; *Kpne*, *Klebsiella pneumoniae*; *Eclo*, *Enterobacter cloacae*; *Kcry*, *Kluyvera cryocrescens*; *Sfle*, *Shigella flexneri*; *Eco*, *Escherichia coli*; *Neur*, *Nitrosomonas europaea*; *Nmen*, *Neisseria meningitides*; *Bfun*, *Burkholderia fungorum*; *Rsol*, *Ralstonia solanacearum*; *Rmet*, *Ralstonia metallidurans*.

thi) *recA56*::Tn*10 srl fis*::*767 λ*[DE3] F′pro *lacI*^{SQ} Z_{u118} Tn*5*), and the mutations were verified by DNA sequencing using alkali-denatured plasmid DNA and Sequenase version 2.0 (U.S. Biochemicals) as specified by the supplier.

WT and mutant FIS proteins were overexpressed in *E. coli* strain RO845 by induction with 0.2 mM isopropyl β-D-thiogalactoside (IPTG) for 1 h and purified as previously described (*46*). The mutations were verified through electrospray ionization (positively charged ion mode) mass spectra obtained on an Agilent 1100 series LC/MSD system (Palo Alto, CA). Samples were introduced into the ion source using a syringe pump at a flow rate of 7 μL/min or using the autosampler. In the latter case, samples (5−10 μL) were injected into the flow (200 μL/min) of a 50:50 mixture of acetonitrile with 0.2% formic acid.

Structure and Sequence Analysis. Four FIS crystal structures were compared for all discussions about the environment of the tyrosine residues: 3FIS (*47*), 1FIA (*48*), 1F36 (*49*), and 1ETY (*43*). The solvent-exposed surface area was determined using the accessible surface calculation package available at http://mendel.imp.univie.ac.at/mendeljsp/index.jsp (*50*, *51*), which uses a probe size of 1.4 Å (IMP Bioinformatics Group, Vienna, Austria). The backbone atoms were not included since the conservative nature of the Tyr to Phe mutation is not expected to alter the backbone arrangement. Sequences homologous to the *E. coli* FIS sequence were identified in a Blast search (*52*) that resulted in 34 additional bacterial FIS sequences. The sequences were aligned using MultAlin (*53*), available at http://prodes.toulouse.inra.fr/multalin/multalin.html.

Sample Preparation. FIS concentration (in monomer units) was obtained in 1 M NaCl and 25 mM tris(hydroxymethyl)-aminomethane hydrochloride (Tris-HCl) at pH 7.0, using an extinction coefficient at 278 nm of 6340 M^{-1} cm^{-1} for WT, 4475 M^{-1} cm^{-1} for Y38F, 4670 M^{-1} cm^{-1} for Y51F, 4742 M^{-1} cm^{-1} for Y69F, and 4480 M^{-1} cm^{-1} for Y95F, determined using a previously described method (*54*). Unless otherwise stated, all experiments were performed using 36 μM FIS at 20 °C in 10 mM potassium phosphate buffer (PB) at pH 7.2 with 0.1 M NaCl. Urea concentrations for all experiments were determined from the refractive index, measured using an Abbe refractometer (*55*).

DNA Binding Assay. Varying amounts of purified preparations of WT or mutant FIS proteins were incubated with 1 fmol of the ^{32}P-end-labeled 430 base pair (bp) DNA fragment, containing the distal FIS binding site of the recombinational enhancer involved in the *Salmonella typhimurium* Hin-mediated DNA recombination reaction (*56*) in 20 μL of binding buffer (20 mM Tris-HCl, pH 7.5, 10 mM EDTA, 80 mM NaCl, 10 μg/mL sonicated salmon sperm DNA). After the mixture was incubated for 10 min at room temperature, 5 μL of gel loading buffer (binding buffer made

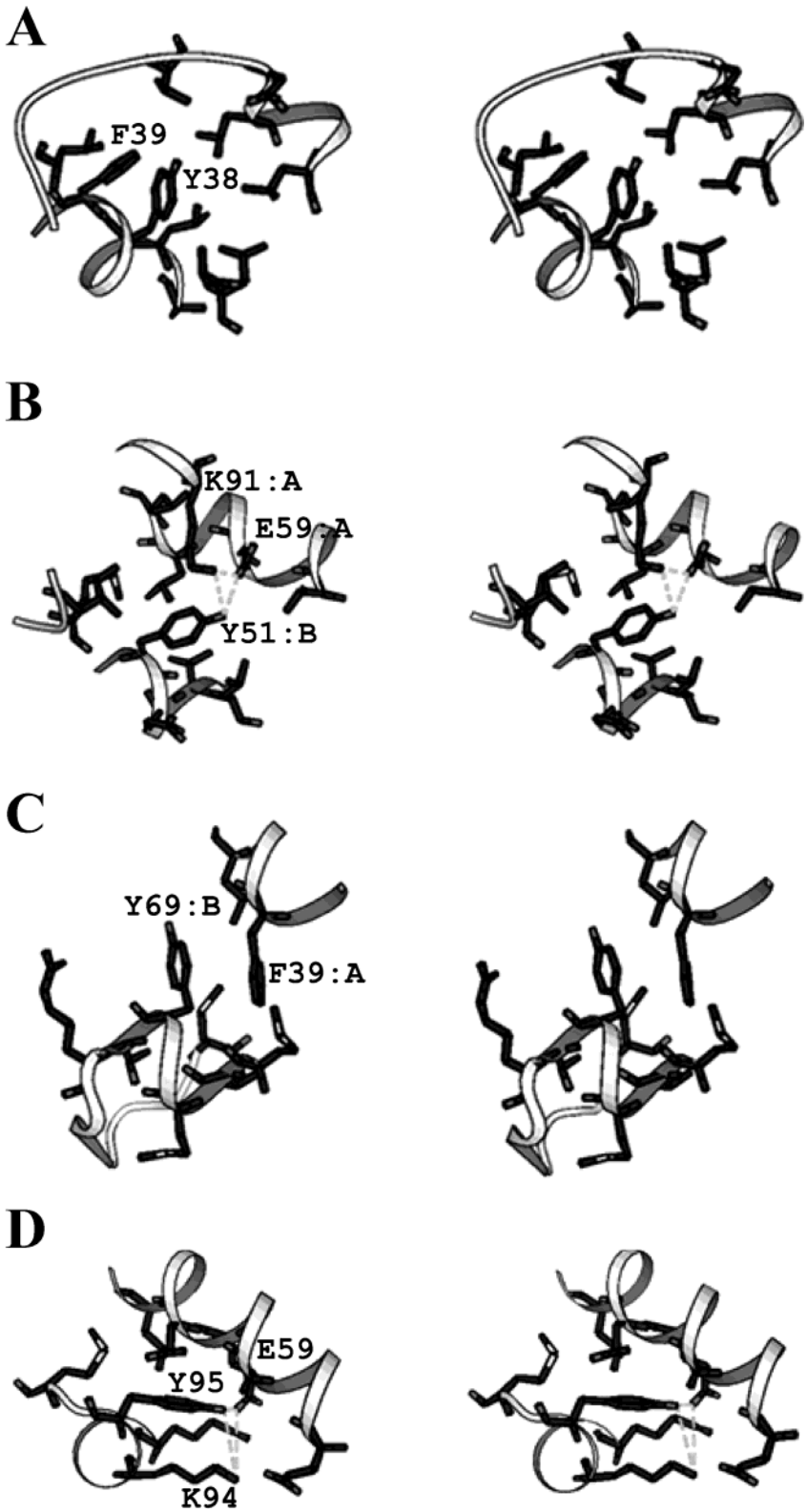

FIGURE 3: Stereoview structures demonstrating the environment around each of the tyrosine residues in WT FIS, Y38 (A), Y51 (B), Y69 (C), and Y95 (D). Each residue is being viewed from the solvent-exposed face or edge. Labeled residues highlight interacting residues proposed to be key to each tyrosine and are labeled as from chain A or B when intermolecular interactions are involved. The broken lines represent hydrogen bonds. The figure was prepared using the 1FIA (*42*) and 1ETY (*43*) FIS structures and drawn with MOLSCRIPT (*89*).

to 7.5% Ficoll and 0.1% bromophenol blue) was added to each sample, and the resultant mixture ws immediately loaded onto a 8% acrylamide−bisacrylamide (60:1) gel in TBE buffer (0.089 M Tris−borate, pH 8.3, 2.5 mM EDTA). Electrophoresis was performed at 2.0 mA/cm for 5 min and then at 1.6 mA/cm for 3 h. The intensities of DNA signals on the gel were measured using a Storm 860 PhosphoImager and ImageQuant software (Molecular Dynamics, Inc., Sunnyvale, CA). The percentage of bound DNA fragments was plotted against the molar FIS concentration and used to obtain the dissociation constant (K_d), defined as the concentration of FIS required to achieve 50% DNA binding. For each FIS

protein analyzed, the results from four separate binding assays were combined in one curve and fitted with KaleidaGraph v.3.5 software using the equation $Y = [FIS]/([FIS] + K_d)$, where Y is the fraction of bound DNA.

Circular Dichroism. Circular dichroism (CD) spectra were recorded on an OLIS CD instrument (Bogart, GA) equipped with a dual beam optical system. Equilibrium urea denaturations in the far-ultraviolet (far-UV) were monitored at 222 nm, and 250 nm was used for baseline correction. Samples were prepared independently at each urea concentration, and the signal was measured after equilibrating for at least 4 min, which is sufficient time to achieve equilibrium (*44*). Equilibrium was confirmed by obtaining the same results when preparing the FIS samples using a codilution method, as previously described (*44*), and from kinetic refolding and unfolding experiments (data not shown) in urea, which show that 4 min is sufficient time for the unfolding and refolding reactions to be complete. Full wavelength scans in the near-UV were taken from 315 to 250 nm. Far-UV CD denaturations were performed in a 0.1 cm cell, while near-UV CD data were collected using a 2 cm cell in order to obtain sufficient signal to accurately observe the near-UV signal.

Fluorescence and Fluorescence Anisotropy. Intrinsic fluorescence and fluorescence anisotropy measurements were performed on a Hitachi F-4500 fluorescence spectrophotometer (Tokyo, Japan) at 20 °C using a 1 cm path length cuvette. Full wavelength scans were taken from 285 to 360 nm using an excitation wavelength of 276 nm. The excitation and emission slits were set to have a 5 nm band-pass through the monochromators. Scans of unfolded FIS were obtained using samples containing 10 mM PB (pH 7.2) and 5.5 M urea.

Steady-state fluorescence and fluorescence anisotropy were used to observe the urea-induced equilibrium denaturations of WT and Y → F FIS, monitoring the emission at 305 nm. The denaturations were performed by a codilution method (*44*), in which FIS samples of progressively higher urea concentrations were made by repetitive withdrawal from a FIS sample (originally in 0 M urea) in the cell followed by addition of the same volume of an unfolded FIS solution (7−9 M urea). Each sample was equilibrated for 4 min prior to recording the signal. For each fluorescence anisotropy value, at least five measurements were recorded and averaged. The integration time was 1 s. Fluorescence anisotropy was calculated from the formulas:

$$A = \frac{I_{vv} - GI_{vh}}{I_{vv} + 2GI_{vh}} \quad (1)$$

$$G = I_{hv}/I_{hh} \quad (2)$$

where I_{vv}, I_{vh}, I_{hh}, and I_{hv} are the fluorescence intensities when the excitation and emission polarizers, respectively, are set in the vertical (v) or horizontal (h) positions (*57*). The fluorescence anisotropy urea denaturations were not analyzed taking into account the quantum yield change upon unfolding, since we do not know the exact quantum yields of the native and unfolded states of FIS. Nevertheless, due to the very low signal change (only 25−50%) upon unfolding of WT FIS and the Y → F FIS mutants, the effect of quantum yield changes on the fluorescence anisotropy should be minimal, as shown by Eftink (*46*). Urea denaturations performed using steady-state fluorescence were taken for qualitative purposes only, due to the steep baselines seen for some of the FIS proteins (*46*).

Limited Proteolysis. Limited trypsin proteolysis was carried out on WT and the Y → F FIS mutants at 20 °C using a trypsin to protein ratio of 1:500 (w/w). Trypsin [L-1-tosylamido-2-phenylethyl chloromethyl ketone (TPCK) treated] was purchased from Sigma (St. Louis, MO). A sample was made containing 36 μM FIS in reaction buffer (25 mM Tris-HCl, 1 mM ethylenediaminetetraacetic acid, pH 7.6) (*58*). Trypsin was diluted into reaction buffer from a concentrated stock (stored frozen in 0.01 M HCl) and added to the FIS sample. Aliquots were removed at times ranging from 0 to 500 min.

Limited proteolysis with V8 protease (ICN Pharmaceuticals, Irvine, CA) was performed at a 1:1 (w/w) protease to protein ratio. One reaction sample was made containing 27 μM FIS in 25 mM Tris-HCl and 0.2 M NaCl, pH 8.0. V8 protease was added directly from stock protein stored frozen in water, and V8 proteolysis was carried out for over 100 h. The trypsin and V8 protease cleavage reactions were stopped by mixing 1:1 (v/v) with sodium dodecyl sulfate−polyacrylamide gel electrophoresis (SDS−PAGE) sample buffer, boiling for 5 min, and then freezing the samples (−20 °C) until ready to run on a 16% tricine SDS−PAGE gel. All proteolysis experiments were conducted on WT and the Y → F FIS mutants at the same time, using the same reaction buffers and protease samples for each mutant, to be internally consistent and minimize error in the results, especially for the experiments involving the V8 protease.

Proteolyzed FIS samples were also analyzed using matrix-assisted laser desorption ionization (MALDI) mass spectrometry (MS) as previously described (*44*). The MS samples were reacted exactly as described above, but the reactions were stopped by addition of trifluoroacetic acid (TFA) to a final concentration of 0.2% (v/v) and then boiled. Samples were desalted and concentrated using Millipore brand ZipTips (Bedford, MA).

Data Modeling. For comparison of data collected from the different mutants, the data were internally normalized using the formula:

$$(Y_o - Y_n)/(Y_u - Y_n) \quad (3)$$

where Y_o is the signal at a given urea concentration and Y_n and Y_u are the first and last data points, respectively. By using this method of normalization, we were able to preserve the original baseline slopes.

The data from the urea denaturation experiments were fit to a two-state dimer model, with native dimer (N_2) in equilibrium with unfolded monomers (2U):

$$N_2 \leftrightarrow 2U \quad (4)$$

The equilibrium constant, K_u, is defined as $K_u = [U]^2/[N_2]$. Since the measured signal is proportional to the fraction of native (F_n) and unfolded (F_u) protein, it can be expressed as

$$Y_o = Y_n(1 - F_u) + Y_u(F_u) \quad (5)$$

where F_u is determined as previously described (*44*). Equation 5 was used to fit the denaturation data to obtain the thermodynamic parameters listed in Table 2. K_u was defined according to the linear free energy model, which

states that the changes in free energy (ΔG_u) that accompany protein unfolding are linearly dependent on the concentration of denaturant (*59, 60*):

$$\Delta G_u = -RT \ln K_u = \Delta G_{H_2O} - m[\text{denaturant}] \quad (6)$$

The baseline slopes and intercepts were used as fitting variables as shown in eq 5, in addition to m and ΔG_{H_2O}. Fits of individual data sets to the two-state model were performed with KaleidaGraph v.3.5 (Synergy Software). The difference in ΔG_u between the WT and mutant FIS proteins was calculated as previously described (*61*, *62*):

$$\Delta\Delta G_{H_2O} = \langle m \rangle \Delta C_m \quad (7)$$

where $\langle m \rangle$ is the average value of m.

The deconvolution of the contribution of each tyrosine residue to the net fluorescence signal of WT FIS was taken from data gathered on the same day to have the most reliable comparison between the signals from WT FIS and the Y → F FIS mutants. The raw fluorescence data were divided by the first point (0 M urea) to internally normalize the data. The data were then fit to the two-state denaturation model, and the results were used to obtain a uniform fluorescence denaturation profile for each protein. The contribution of Tyr95, Tyr69, and Tyr38 to the WT FIS signal change was determined by subtracting the corresponding mutant data from the WT FIS data. Due to the dramatic difference in C_m between WT and Y95F FIS, in order to subtract the Y95F FIS data from that of WT FIS and have the deconvolution accurately represent the Tyr95 contribution to the WT fluorescence signal, the Y95F FIS data were translated such that the C_m matched that of WT FIS. Such adjustments were not necessary for the Y69F FIS data, because the C_m is the same as WT FIS, or for the Y38F FIS data, because the signal change is nearly identical to WT FIS (Figure 6). Since the Y51F FIS mutation appears to be influencing the fluorescence of other tyrosine residues, we avoided direct subtraction of the Y51F FIS signal from that of the WT to obtain the fluorescence contribution from Tyr51. Therefore, the contribution of Tyr51 was determined by subtracting the combined contribution of the other tyrosine residues from the WT FIS data. These calculations can be confirmed by summing the fluorescence signal contribution of each tyrosine residue, which results in the WT FIS denaturation profile.

RESULTS

DNA Binding Affinity. The C and D helices of FIS form a helix−turn−helix DNA binding motif that is required for DNA binding (*63*). Mutations of residues in this region required for DNA binding (e.g., R85H, T87A, R89C), or residues critical for native state stability (e.g., E59K), generally result in severe reduction (>200-fold) of DNA binding affinity (ref *63* and unpublished results). Of the four tyrosines, only Y95 is located in the DNA binding region (helix D, Figure 1) but is not expected to be involved directly in DNA binding. Thus, effects of Y → F replacements on DNA binding activity are likely to reflect changes in the structure of the protein. DNA binding reactions were conducted with the WT and each of the four Y → F mutants using a 430 bp DNA fragment containing a FIS binding site used in stimulation of DNA inversion in *S. typhimurium* (*56*). The results show that Y38F and Y69F bind DNA with affinities comparable to that of the WT protein (Table 1), suggesting that their overall effect on the native structure may be minimal. The Y95F and Y51F mutant proteins showed a moderate reduction in DNA binding affinity (3.8- and 8.5-fold, respectively), suggesting the existence of small, but perceptible, structural alterations in the C-terminal region of these mutant proteins. These observations suggest that the four Y → F mutant proteins have three-dimensional structures very similar to that of WT FIS and that slight changes in the packing of the mutant proteins may be causing the small differences in DNA binding affinities.

Table 1: WT and Mutant FIS−DNA Binding Activities

protein	DNA binding K_d (nM)[a]
WT	4.0 ± 0.8
Y95F	15.3 ± 2.7
Y69F	3.6 ± 1.8
Y51F	34.1 ± 5.7
Y38F	5.4 ± 0.7

[a] DNA binding affinity (K_d) was measured using a gel mobility shift assay on a DNA fragment containing the Hin recombinational enhancer distal Fis binding site. Errors are based on the fit of the average of data from four individual experiments.

Equilibrium Denaturation Experiments. The urea-induced denaturations of the Y → F FIS mutants were monitored using far-UV CD and steady-state fluorescence anisotropy (Figure 4) and compared to that observed for WT FIS (*46*). The denaturation transitions all demonstrated concerted, concentration-dependent behavior (data not shown), and the m-values of the Y → F FIS mutants were constant with varying protein concentration (data not shown), which is a requirement for defining an oligomeric protein as having a two-state equilibrium denaturation mechanism (*44*). Therefore, the urea denaturation transitions were fit to the two-state model, $N_2 \leftrightarrow 2U$ (Figure 4). Indeed, the agreement between the C_m and m-values between the far-UV CD and fluorescence anisotropy data (Table 2) further demonstrates that the equilibrium denaturation of Y69F, Y51F, and Y38F FIS is a two-state process. However, there is a significant discrepancy in the m-value seen for Y95F FIS by fluorescence anisotropy compared to that observed by far-UV CD (Table 2), which points to a possible intermediate. Minor inconsistencies between the fluorescence anisotropy and far-UV CD data could be due to the use of intrinsic fluorophores for the anisotropy measurements (*46*, *57*). Thus, the far-UV CD data were taken to be the most reliable measurement of stability. The data show that while the surface-exposed Y69F mutation had no effect on stability (Table 2 and Figure 4), the Y38F mutation, which removes a tyrosine residue buried in a hydrophobic pocket, resulted in an increase in stability of 1 kcal/mol (Table 2). Y51F and Y95F FIS, which are involved in a complex hydrogen-bonding network in the C-terminus of FIS, are destabilizing mutations that result in a loss of 0.7 and 1.8 kcal/mol in stability, respectively (Table 2).

It should be noted that the $\Delta\Delta G_{H_2O}$ values in Table 2 were calculated from eq 7, using the average m-value between WT FIS and each Y → F FIS mutant. If, instead, the $\Delta\Delta G_{H_2O}$ values for Y51F FIS are calculated by subtracting the ΔG_{H_2O} determined using eq 6, Y51F FIS would have a $\Delta\Delta G_{H_2O}$ of

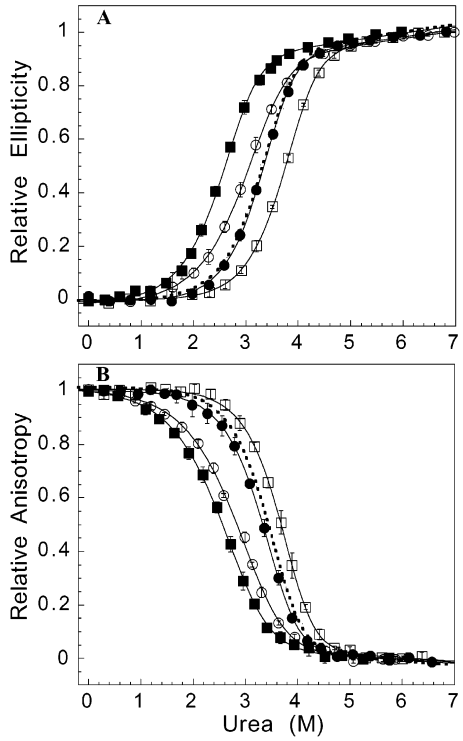

FIGURE 4: Urea-induced denaturation of Y → F mutant FIS monitored by (A) far-UV CD and (B) steady-state fluorescence anisotropy. The data were internally normalized as described in Materials and Methods. The denaturations were performed at 36 μM for Y95F (■), Y69F (●), Y51F (○), and Y38F (□). The dashed lines indicate the urea denaturation transition of WT FIS at 36 μM (*46*). Error bars represent the standard deviation from an average of at least three individual data sets. The solid lines on the denaturation curves indicate a two-state fit of the data as described in Materials and Methods.

Table 2: Thermodynamic Analysis of the Equilibrium Denaturation of FIS Based on a Two-State Model[a]

method	protein	C_m (M urea)	*m*-value [kcal/(mol M)]	$\Delta\Delta G_{H_2O}$[b] (kcal/mol)
far-UV CD	WT	3.27 ± 0.02	2.37 ± 0.09	
	Y95F	2.50 ± 0.02	2.23 ± 0.10	−1.77 ± 0.12
	Y69F	3.29 ± 0.01	2.46 ± 0.03	+0.06 ± 0.06
	Y51F	2.94 ± 0.01	1.97 ± 0.04	−0.72 ± 0.06
	Y38F	3.70 ± 0.01	2.43 ± 0.06	+1.05 ± 0.07
fluorescence anisotropy	WT	3.43 ± 0.02	2.40 ± 0.12	
	Y95F	2.50 ± 0.03	1.67 ± 0.03	−1.89 ± 0.14
	Y69F	3.30 ± 0.02	2.41 ± 0.12	−0.31 ± 0.10
	Y51F	2.88 ± 0.04	1.96 ± 0.12	−1.20 ± 0.14
	Y38F	3.66 ± 0.02	2.51 ± 0.09	+0.56 ± 0.08

[a] Urea denaturation profiles were analyzed according to the linear free energy model. Errors for *m* and C_m were from a weighted fit of the average data from at least three individual experiments. The protein concentration was 36 μM. [b] $\Delta\Delta G_{H_2O} = \langle m \rangle \Delta C_m$, where $\langle m \rangle$ is the average value of *m* (*61*, *62*). The $\Delta\Delta G_{H_2O}$ errors were calculated by compounding the error from the individual *m* and C_m values.

2.0 kcal/mol (using the far-UV CD data). Due to the sensitivity of the *m*-value to small errors (*64*), we decided to use the average *m*-value (eq 7) to calculate the $\Delta\Delta G_{H_2O}$ data in Table 2. However, due to the large difference in *m*-value between Y51F and WT FIS, the use of this method could significantly underestimate the $\Delta\Delta G_{H_2O}$ (*65*) of the Y51F FIS mutant. Therefore, it is likely that the destabilization of FIS due to the Y51F mutation is somewhere between 0.7 and 2 kcal/mol.

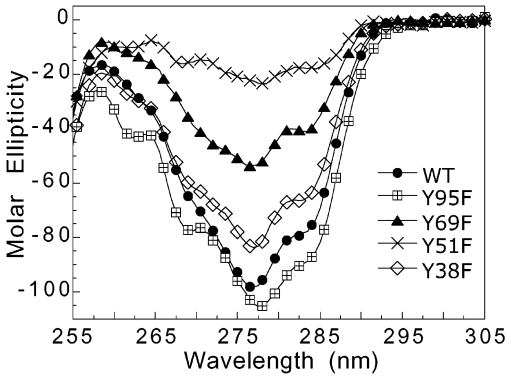

FIGURE 5: Representative near-UV CD spectra of WT and the Y → F FIS mutants from 305 to 255 nm. Molar ellipticity has units of deg·cm²·dmol⁻¹.

Changes in Fluorescence and Near-UV CD Signals. The absence of tryptophan residues and the variable locations of four tyrosine residues make FIS a good system for examining the contribution of each tyrosine to the near-UV CD and fluorescence signals. The near-UV CD spectra of WT FIS and each of the Y → F FIS mutants are shown in Figure 5. The most WT FIS-like spectra are those of Y95F and Y38F FIS, which show slight gains (~3%) and losses (~15%) in signal at 277 nm, respectively, relative to WT FIS. The Y69F and Y51F FIS mutants have significantly decreased near-UV CD signals of about 50% and 80%, respectively. However, the changes in the near-UV CD spectra seen in the Y → F FIS mutants cannot all directly correlate to the individual tyrosine contributions in WT FIS because when the mutant data are subtracted from the WT data, giving the expected contribution from that tyrosine to the WT FIS near-UV CD signal, a summation of these signal contributions results in a near-UV CD spectrum with 35% more signal than that seen in WT FIS. Thus, some structural alteration in one or more of the Y → F FIS mutants must be occurring that alters the environment of at least one other tyrosine residue, resulting in a greater change in signal than is expected due to that particular mutation.

Fluorescence full-wavelength scans in their native and unfolded states and representative urea denaturations of the Y → F FIS mutants (Figure 6) suggest the varying degrees in which each tyrosine residue may contribute to the fluorescence signal of WT FIS. The fluorescence-monitored urea denaturations were not fit to extract of thermodynamic parameters, due to the large baseline signal changes caused by the tyrosine fluorescence dependence on urea (*57*) and the nonsigmoidal shapes of some of the curves (Figure 6). The urea denaturation profiles of the Y → F FIS mutants (Figure 6B) are shown to demonstrate the contribution of each tyrosine to the fluorescence signal change in WT FIS, which is not apparent by simply looking at the full-wavelength scans (Figure 6A) or analyzing the 3D structure of FIS. The intensities of the Y38F FIS native and unfolded spectra are consistent with the expected 25% decrease in the total fluorescence signal compared to WT FIS (Figure 6A). Yet, the fluorescence unfolding profile of Y38F FIS is almost identical to WT FIS (Figure 6B), with only ~20% increase in signal at 5.5 M urea. This suggests that Tyr38 does not contribute significantly to the urea-induced denaturation transition of WT FIS. In Y69F FIS, there is a much smaller increase in signal intensity (~7%) upon unfolding with urea

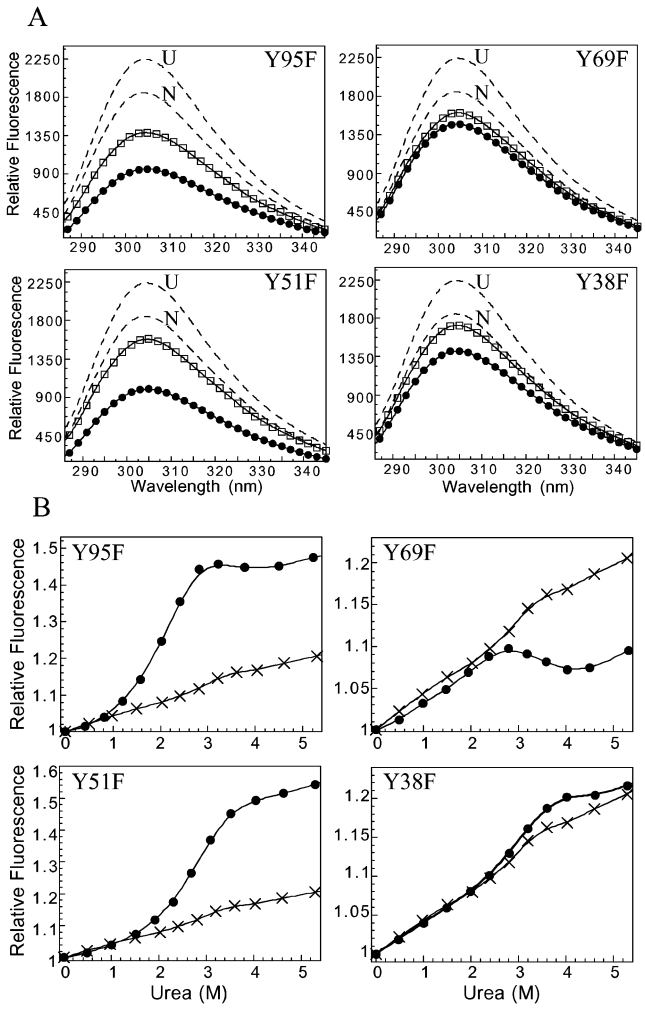

FIGURE 6: Fluorescence emission spectra (A) of the Y → F FIS mutants scanned from 285 to 350 nm with an excitation wavelength of 276 nm. The proteins were equilibrated under native (●) conditions or unfolded in 5.5 M urea (□). The native (N) and unfolded (U) spectra of WT FIS are shown as dashed lines. A representative urea denaturation profile (B) of each Y → F mutant is shown (●) overlaid with WT FIS data (×). The denaturations were performed by monitoring the fluorescence emission at 305 nm. The solid lines through the data do not represent a specific fit and are shown only to highlight the shape of the denaturation curves.

than seen for WT FIS (Figure 6A), and therefore, the denaturation transition profile also differs notably from WT FIS (Figure 6B). Although it has the steep baseline slope observed for WT FIS, the signal change in the transition region goes in the opposite direction than that observed with WT FIS. The loss in signal change upon unfolding caused by the Y69F mutation indicates that Tyr69 is an important contributor to the signal change seen in the fluorescence denaturation profile of WT FIS.

Interestingly, the Y95F and Y51F mutations result in very similar changes to the fluorescence of FIS (Figure 6A), each having a much lower signal in the native state than would be expected if each tyrosine contributed one-fourth of the total WT FIS signal. This implies that, in WT FIS, Tyr95 and Tyr51 both contribute significantly to the native state fluorescence. The signal increases upon unfolding for Y95F and Y51F FIS are about 1.4- and 1.5-fold, respectively, which is much greater than what is observed for WT FIS (Figure 6B). This dramatic increase in the total signal change upon unfolding combined with the lower native state signal of Y95F and Y51F FIS implies that, in WT FIS, both Tyr95 and Tyr51 are more fluorescent in the native state and their signals are quenched upon unfolding. However, it is not possible to combine these data directly with the contribution from Tyr69 and Tyr38 to obtain a WT-like denaturation profile. Therefore, as seen for the near-UV CD, one or more of the Y → F FIS mutants must alter the environment and fluorescence of at least one of the three remaining tyrosine residues in that mutant.

Limited Proteolysis by Trypsin and V8 Protease. Limited proteolysis by trypsin and V8 protease was used to examine changes in the conformational dynamics that may have resulted from the Y → F mutations. Trypsin cleaves at arginine and lysine residues, which are concentrated in the C and D helices that make up the C-terminus of FIS (Figure 2). However, FIS has no trypsin cleavage sites between residues 36 and 71, which is the majority of the dimer core. In contrast, V8 protease cleaves at aspartic and glutamic acid residues, of which there are six between residues 36−71 but none after residue 64 (Figure 2). Therefore, trypsin is mainly probing the C-terminus while V8 probes the dimer core involving the A and B helices.

The trypsin-generated proteolytic fragments of FIS (Figure 7A) were analyzed by MALDI-MS, and their masses were confirmed to be equal to those previously observed for FIS (*44*). WT and Y69F FIS show similar trypsin proteolysis patterns, as might be expected due to their equal stability (Table 2). The C-terminus of Y38F FIS is cleaved somewhat faster than WT FIS to the main fragments 6−76 and 6−71 (*44*) observed in the gel (Figure 7A) even though Y38F FIS is a little more stable than WT FIS (Table 2). Y95F and Y51F FIS both show a marked increase in their susceptibility to trypsin proteolysis over WT FIS, consistent with their decreased stability (Table 2), but Y51F FIS is slightly more susceptible to cleavage than Y95F FIS.

Limited proteolysis using V8 protease (Figure 7B), unlike trypsin, showed that the proteolytic susceptibility of the Y → F FIS mutants correlated well with the stability data shown in Table 2. WT and Y69F FIS exhibit nearly identical cleavage patterns (Figure 7B). MALDI-MS showed the major fragments observed on the gels (Figure 7B) to be 4−59 (∼6000 kDa), 65−98 (∼4000 kDa), and 30−52 (2500 kDa) (data not shown). The native state of the more stable Y38F FIS mutant is cleaved somewhat slower and does not seem to populate the small fragments seen in WT and Y69F FIS. The dimer cores of Y95F and Y51F FIS are cleaved much faster than the other two mutants or WT FIS, consistent with their relative stability (Table 2).

DISCUSSION

The Y → F FIS mutants have been used to gain a better understanding of the role of the various tyrosine residues on DNA binding, stability, and flexibility and for deconvoluting the individual contribution of each tyrosine to the spectroscopic signals of WT FIS. It is important to note that crystal structures of these mutants are not available and disruption of local native structure upon mutation must be considered (*7*, *8*). However, the virtually identical far-UV CD spectra (data not shown) and the conservative nature of these mutations suggest only minor disruption of the native

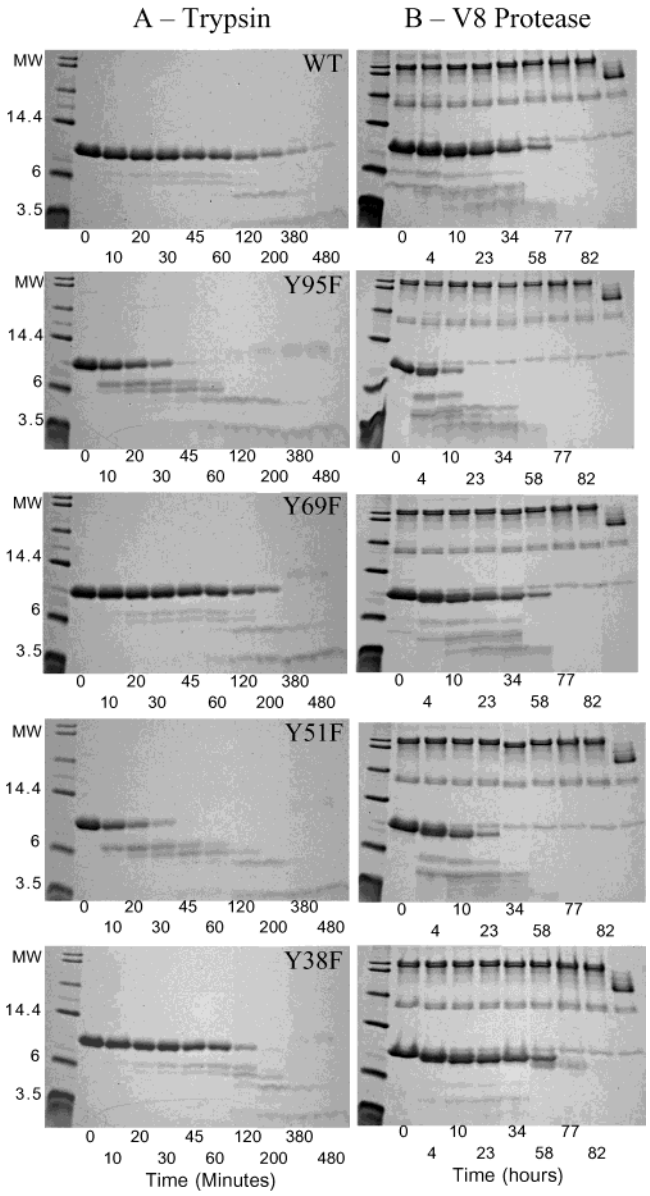

FIGURE 7: Limited trypsin cleavage of WT and Y → F FIS mutants at 20 °C, using trypsin (A) and V8 protease (B) at a 1:500 and 1:1 (w/w) protease:protein ratio, respectively. These gels are from a representative experiment in which all reactions were carried out on the same day as described in Materials and Methods. Aliquots from reacting samples were removed and the reactions stopped at the times indicated below the gels. The last lane on the V8 protease gels (B) is a control of V8 protease that was incubated without FIS for 82 h.

state (*65*, *66*). This is supported by the DNA binding experiments (Table 1), which show that all four mutants have the necessary native structure to enable high-affinity binding ($K_d \sim 3.6-34$ nM) to a DNA fragment carrying a FIS binding site. The mutants Y38F and Y69F showed binding affinities that were comparable to that of the WT FIS, while Y95F and Y69F showed moderate reductions in binding affinity (3.8- and 8.5-fold, respectively), suggesting that minor alterations in the structure or dynamics of the C-terminal region (required for DNA binding) might have occurred in the latter mutants. The structure around each tyrosine residue in FIS (Figure 3) also supports the idea that their conservative mutation to phenylalanine should not affect the global protein structure (*67*) but only the local environment around the mutated residue. Thus, each Y → F FIS mutant should provide fairly reliable information about the contribution of the tyrosine residues to the stability, flexibility, and near-UV CD and fluorescence properties of WT FIS.

Tyrosine Hydrogen Bonding: Local Dynamics Effects. Traditionally, the use of limited proteolysis for monitoring protein flexibility and dynamics is done using a nonspecific protease so that the proteolysis is governed by the protein dynamics and not the protease specificity (*68*). However, through the use trypsin and V8 protease we have been able to separately observe the unfolding/dynamics of the FIS C-terminal DNA binding domain (helices C and D) and dimer core (helices A and B), respectively. While the relative rates of proteolysis are consistent within each experiment, the actual cleavage rates from the V8 proteolysis were not consistent between different experiments, perhaps as a result of the very long incubation times. Although it would be ideal to show kinetic plots demonstrating the differences in cleavage rates between WT and the Y → F FIS mutants, due to the difficulties in analyzing the V8 data, we only show the gels and focus on the relative rate differences. Nevertheless, the results from V8 proteolysis were always internally consistent and correlate directly with the stability of FIS (Table 2), showing the rates of cleavage to be Y38F < WT ≈ Y69F < Y51F < Y95F (Figure 7). FIS has six cleavage sites (aspartic and glutamic acid) for V8 protease in helices A and B, which make up the hydrophobic core of FIS. Thus, since V8 protease is likely to cleave globally unfolded FIS transiently populated due to its $N_2 \leftrightarrow 2U$ equilibrium, the rate of proteolysis should relate directly to the ΔG_{H_2O} (*69*), which is what we observed.

When trypsin is used in the proteolysis experiment, the cleavage rates (WT ≤ Y69F < Y38F ≪ Y95F < Y51F) do not correlate with stability: Most of the trypsin cleavage sites (arginine and lysine) occur within the C-terminal DNA binding domain, with no cleavage sites from residue 36 to residue 71, which is most of the dimer core. Therefore, trypsin proteolysis is mainly monitoring the local unfolding or flexibility of the C-terminus of FIS, which may not necessarily correlate with overall protein stability. It is interesting that Y38F FIS has a more exposed C-terminus than WT FIS given that it is the tyrosine furthest away from that region. The Y51F and Y95F FIS mutants are highly susceptible to trypsin proteolysis, with a rate that appears to be faster, relative to WT FIS, than that seen when using V8 protease. Although the increased exposure of the C-terminus observed for Y51F and Y95F FIS is partially due to the decreased stability of the protein, the fact that their relative rates are faster than seen in V8 proteolysis and that they do not correlate with their respective stability (Table 2) leads us to believe that the observed difference in proteolysis is partially due to an increase in dynamics. This is supported by trypsin proteolysis data from the FIS mutant P61A that show a dramatic increase in the rate of proteolysis at the C-terminus, even though the mutation stabilizes FIS by 4 kcal/mol (*44*). In the case of P61A FIS, the crystal structure (*70*) suggests that a slight repacking of the B-helix resulted in the disruption of a hydrogen bond and salt bridge network in the C-terminus (*44*). Therefore, the increase in C-terminal flexibility seen for Y51F and Y95F FIS is not surprising, considering they are directly involved in this complex

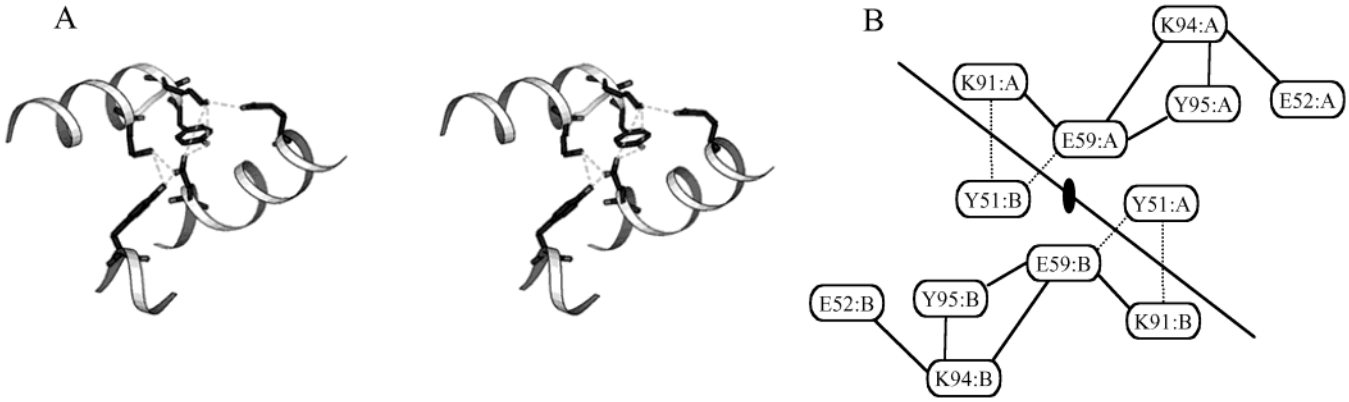

FIGURE 8: Illustration of the hydrogen-bonding/salt bridge network around Tyr95 and Tyr51 shown in stereoview (A) and as a schematic representation (B) displayed in the same orientation as in the structural view. The stereoview structure is taken from the 1FIA FIS (*42*) and drawn with MOLSCRIPT (*89*). The schematic has each residue labeled with A and B to designate which subunit the residue is on. Inter- and intramolecular interactions are designated by dashed and solid lines, respectively. The line drawn through the schematic representation separates the two FIS subunits, and the symmetry axis is shown by an oval.

electrostatic network (Figure 8). It is possible that the effects on the flexibility of the C-terminus could account for the high sequence conservation of the tyrosine residues Y95 and Y51 (Figure 2). Similar effects on protein flexibility due to mutations have been seen for the Trp repressor DNA binding domain (*71*).

Tyrosine Hydrogen Bonding: Effects on Stability and Denaturation Mechanism. The urea-induced equilibrium denaturations of Y69F and Y38F FIS clearly demonstrate that they unfold in a concerted two-state fashion (Table 2, Figure 4) as seen for WT FIS (*46*). Y69F FIS shows no change in stability upon mutation (Table 2) even though removal of a solvent-exposed polar group usually results in a small decrease in stability (*10*). The intermolecular ring stacking interaction between Tyr69 and Phe39 (Figure 3C), which may have a stabilizing effect (*72*, *73*), should be preserved in Y69F FIS and should also have a helix propensity (*74*) similar to that of the WT FIS sequence.

The Y38F mutation results in an increase in stability (Table 2). This is consistent with previous work showing that the burial of a polar group lacking a hydrogen-bonding partner (Figure 3A) is destabilizing (*3*, *6*, *7*, *67*). While tyrosine residues can be stabilizing over phenylalanine, due to the formation of hydrogen bonds (*8*−*10*), protein stabilization of phenylalanine over tyrosine has been observed (*8*, *10*, *18*, *75*, *76*). As seen in Y38F FIS, stabilizing phenylalanine mutants seem to occur at positions where favorable hydrogen bonds are not formed and hydrophobic stabilization dominates (*3*, *10*, *76*).

Y51F FIS also demonstrates a concerted two-state denaturation mechanism, but it is a destabilized mutant (Table 2, Figure 4) with a modest decrease in *m*-value compared to WT FIS (Table 2). It is worth noting that the $\Delta\Delta G_{H_2O}$ of Y51F (0.7 kcal/mol) calculated on the basis of the averaging of *m*-values (Table 2) is a lower limit of the destabilizing effect of the mutation, as the $\Delta\Delta G_{H_2O}$ would be about 2.0 kcal/mol if the *m*-value of Y51F FIS were used directly to determine the stability of the protein. Regardless, since no deviation in two-state behavior is observed, the decrease in *m*-value points to a difference in the solvent-accessible surface area between Y51F and WT FIS in either the native or unfolded state (*77*). This decrease in *m*-value may be a result of the break of the intermolecular interactions Y51F makes with Glu59 and Lys91 (Figures 3B and 8). Considering the central role of Glu59 in the electrostatic network, the disruption of this interaction may have a significant effect on the dynamics of the C-terminus, leading to increased solvent exposure in the native state.

Y95F FIS shows the greatest deviation from the WT FIS denaturation profile and stability. The data in Table 2 show that Y95F is a destabilizing mutation and has the lowest C_m of all the Y → F FIS mutants. However, the *m*-value obtained for Y95F FIS by fluorescence anisotropy is drastically lower than that obtained by far-UV CD (Table 2), which could indicate the presence of an equilibrium folding intermediate. The presence of an intermediate for Y95F FIS is supported by the fluorescence-monitored urea denaturation of Y95F FIS (Figure 6B), which completes its transition well before the CD and fluorescence anisotropy data. The fluorescence data were not analyzed to obtain thermodynamic parameters due to the nonsigmoidal nature of the transition, which makes it difficult to properly fit and interpret the data. The Y95F mutation is expected to affect the C-terminal region, where it is involved in the complex hydrogen-bonding/salt bridge network (Figures 3D and 8). One reason that Y95F FIS may be more prone than Y51F FIS to form an equilibrium intermediate is that the former is engaged in intramolecular interactions, whereas Y51F FIS is involved in intermolecular interactions within the electrostatic network (Figure 8). Therefore, the Y51F mutation will most likely destabilize not only the C-terminus but also the monomer−monomer interactions, thereby preserving the concerted denaturation of FIS. By predominantly destabilizing the C-terminus, the Y95F mutation may begin to decouple the intramolecular denaturation of the C-terminus from the intermolecular denaturation of helices A and B. The possibility of an intermediate in the denaturation of Y95F FIS involving the C-terminus is supported by previous data showing that a P61A mutation in FIS stabilizes the C-terminus, but to a lesser extent than the rest of the protein, resulting in an equilibrium denaturation intermediate (*44*).

Functional Importance of Tyrosine Hydrogen Bonding. The DNA binding affinities (K_d) of the four Y → F mutants were similar or moderately reduced (3.4- and 8.5-fold) compared to the WT FIS and suggest that their native structures are not substantially different from that of the WT

protein. The differences observed in DNA binding affinity (Y69F ≈ WT ≈ Y38F > Y95F > Y51F) correlate well with the differences in the dynamics of the C-terminus monitored by trypsin proteolysis, suggesting that the increased flexibility of the C-terminal region may decrease the DNA binding efficiency.

It is not known whether the modest decrease in DNA binding affinity of the Y51F and Y95F FIS may have in vivo consequences. Other mutations in FIS, having up to a 12-fold reduction in DNA binding affinity (e.g., deletion of residues 18−29), did not affect the ability of this protein to stimulate the excision of λ phage DNA from the *E. coli* chromosome (*63*). This indicates that a reduction in DNA binding affinity of this magnitude does not inevitably result in appreciable loss of DNA binding activity in vivo. Mutations resulting in slightly greater loss of DNA binding (∼15-fold) show a moderate decrease in efficiency of stimulation of λ excision from the chromosome. Therefore, the 3.4- and 8.5-fold reduction in DNA binding affinity seen for Y51F and Y95F FIS, respectively, would not be expected to appreciably affect DNA binding activity in vivo, particularly under conditions of bacterial growth in rich medium, which result in very high intracellular levels of FIS during early logarithmic growth phase (*78*). However, it is possible that, under conditions of growth in nutritionally depleted medium, where FIS intracellular levels are much lower, Y51F and perhaps Y95F may show an appreciable reduction in DNA binding in vivo compared to the WT FIS. It is also possible that other functional regions in FIS could be sufficiently affected to diminish one or more of its functions in vivo.

Role of Tyrosines in Near-UV CD and Fluorescence Signals. Figure 5 demonstrates that all of the Y → F FIS mutants alter the near-UV CD spectra from that observed for WT FIS. The minor changes to the near-UV CD spectra due to the Y38F and Y95F mutations imply that these residues are rather mobile in WT FIS. The loss of almost half of the WT near-UV CD signal in Y69F FIS is unexpected from a residue located at the surface, unless it was restricted by some interaction. It is known that aromatic ring interactions give rise to intense near-UV CD spectra (*79*) and Tyr69 is ∼3.9 Å from Phe39 (Figure 3). Thus, the signal lost in Y69F FIS indicates that Tyr69 stacks with Phe39 in WT FIS, thereby contributing to the near-UV CD signal. The Y51F mutation results in a dramatic loss of near-UV CD signal, implying that most of the signal in WT FIS is due to Tyr51. However, the Y51F and Y95F mutations may cause changes in the rotational freedom of other tyrosine residues because Tyr51 and Tyr95 are involved in an extensive hydrogen-bonding network (Figure 8). Thus, while Tyr51 probably makes a significant contribution to the near-UV CD signal, we believe that the Y51F and Y95F mutations may alter the local structure or mobility of the remaining tyrosine residues, resulting in the large loss in the near-UV CD signal in Y51F FIS and the gain of signal seen in Y95F FIS. Although a change in the near-UV CD signal implies loss of structure, studies on the molten globule states of proteins have shown that these states can be characterized as being highly flexible, having no near-UV CD signal, but retaining significant native-like tertiary structure (*80*, *81*). Thus, empirical evidence (*80*, *81*) shows that loss of the near-UV CD signal can arise due to increased flexibility as may occur in some of the Y → F FIS mutants. Therefore, simple deconvolution of the near-UV CD spectra to determine the contribution from each tyrosine was not possible due to the apparent sensitivity of the near-UV CD signal to minor changes in structure (*79*, *82*) and flexibility that could occur around the remaining tyrosines in each Y → F mutant.

WT FIS has a very low fluorescence signal change upon unfolding that is accompanied by steep baseline slopes (*46*). Urea-induced denaturation transitions of the Y → F FIS mutants reveal the influence of each tyrosine residue to the signal patterns observed for WT FIS (*46*). Y38F FIS shows a fluorescence denaturation transition very similar to that of WT FIS (Figure 6B), which suggests that it does not make a significant contribution to the fluorescence signal change of WT FIS upon unfolding. Y69F FIS has a different denaturation profile from WT FIS (Figure 6B), demonstrating the importance of Tyr69 for the net increase in WT FIS fluorescence upon unfolding. It appears that the ring stacking interaction with Phe39 quenches the fluorescence and, therefore, disruption of the ring stacking results in a signal increase upon unfolding. Although there are no reports of Tyr/Phe ring stacking resulting in quenching, ring stacking with DNA base pairs is known to quench tyrosine fluorescence without energy transfer or tyrosine ionization (*83*−*85*). This quenching effect is supported by the near-UV CD data discussed above, demonstrating the signal contribution of Y69 due to the restricted rotation caused by the Tyr69/Phe39 interaction.

The Y95F and Y51F mutations result in a FIS protein that has a much greater signal change upon unfolding (Figure 6B), suggesting that the Tyr51 and Tyr95 signal decreases upon the urea-induced unfolding of WT FIS. However, extracting the contribution of tyrosine residues to the WT fluorescence from the data of Y → F mutants results in a full spectrum with more signal than is actually observed for WT FIS (data not shown). The signal of WT FIS increases about 20% upon unfolding to 5 M urea (Figure 6B), yet Y95F and Y51F FIS each have increases in fluorescence of over 40% (Figure 6). Thus, one or more of the Y → F FIS mutants must be altering the remaining tyrosine residues in the protein such that the spectroscopic signals do not accurately represent the response from mutating the tyrosine in question. In analogy with the near-UV CD data, it appears that Y95F and/or Y51F are responsible for this discrepancy.

Several lines of reasoning and observations point to the Y51F FIS mutant as the most likely mutation causing the disruptions in the FIS protein that result in the discrepancies in near-UV CD and fluorescence signals. First, Y69F FIS should result in no structural changes around the other tyrosines due to its solvent-exposed location. Also, the fluorescence denaturation transition of Y38F shows very little difference from WT FIS. Furthermore, the nearly complete loss of the near-UV CD signal in Y51F FIS suggests that this mutation alters the environment of at least one other tyrosine residue. Tyrosine fluorescence is sensitive to the charge and hydrogen bonding in its local environment (*85*), and therefore, the drastic changes in Y51F FIS fluorescence may arise from alterations in the strength of the hydrogen-bonding interactions around Tyr95 (Figure 8) due to the removal of Tyr51. Thus, we propose that the Y51F mutation translates an effect onto Tyr95 through the hydrogen-bonding

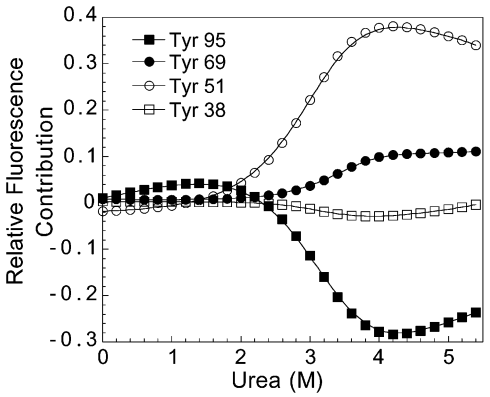

FIGURE 9: The contribution of each tyrosine to the WT FIS fluorescence was deconvoluted from the fluorescence data as described in Materials and Methods.

network in the C-terminus of FIS, causing the observed increase in fluorescence data in Y51F FIS.

The fluorescence profile of the Y → F FIS mutants makes it possible to obtain a rough estimate of the contribution of each tyrosine to the WT FIS fluorescence (Figure 9). This deconvolution was performed on the basis of the assumption that all of the Y → F FIS mutants, except Y51F FIS, were reporting fairly accurately on the fluorescence signal due to the loss of each tyrosine. The Y95F, Y69F, and Y38F FIS fluorescence signals at the various urea concentrations were subtracted from the WT FIS data to determine the signal contribution of each tyrosine residue, and the remaining signal was assigned to Tyr51. The environment-dependent changes in tyrosine fluorescence within the same protein have been seen in other proteins (*20*, *22*). However, the molecular basis for this phenomenon is not clearly understood.

CONCLUSION

The variety of roles that tyrosine residues can play in proteins can be attributed to their twofold hydrophobic and polar nature. The aromatic ring can be involved in hydrophobic and ring stacking interactions while the hydroxyl group can engage in hydrogen bonding. In this study, the contribution of four tyrosine residues to the stability, local dynamics, and spectroscopic properties of FIS was investigated. Such a study had not been done for a small oligomeric protein such as FIS. The lack of tryptophan residues, the presence of four tyrosine residues strategically located within the FIS three-dimensional structure (Figure 1), the diversity of the intra- and intermolecular tyrosine interactions, and the high conservation of these residues (Figure 2) made FIS a compelling model system and were the driving force behind these studies.

Our results have demonstrated the roles of tyrosine residues in three different environments, with the −OH group buried in the protein, exposed on the surface, or in a hydrogen-bonding network. Several general conclusions related to the role of tyrosine residues on FIS stability and dynamics can be made from this study. First, the participation of Y95 and Y51 in the electrostatic network located in the C-terminus contributes a total of about 3 kcal/mol toward the stability of FIS, in agreement with the contribution of tyrosine hydrogen bonding to the stability of monomeric proteins (*8*, *10*) and the importance of hydrogen bond networks for the stability of some proteins (*1*, *9*, *86*). It also appears that, in addition to the stability, the dynamics of the C-terminus is very sensitive to any mutation that alters this network. An increase in flexibility in this region can affect its DNA binding activity (Table 1). It remains to be determined whether this may be the reason for the very high sequence conservation within the C-terminal DNA binding domain (Figure 2). Although DNA binding is only modestly affected by these mutations, their functional significance in vivo cannot be ruled out at present. Second, Tyr38 was found to destabilize FIS by 1 kcal/mol (Table 2). While this effect on stability is expected because of its hydrophobic environment (*3*, *87*), it is intriguing that Y38 is 97% identical among FIS homologues despite its destabilizing effect. The slightly higher susceptibility of Y38F FIS to trypsin proteolysis may suggest that the high conservation of this residue may be related to the need to balance the stability, function, and dynamics of FIS in vivo. Third, as expected for a largely solvent-exposed residue, the Y69F mutation did not alter the stability of FIS. However, since the aromatic residue was preserved, it is possible that the intermolecular aromatic ring stacking between Y69 and F39 may contribute to the stability of FIS.

An attempt was made to deconvolute the contribution of each tyrosine to the fluorescence profile of WT FIS. Due to the lack of a crystal structure for these mutants, it is not clear if any local conformational change may exist, and therefore, our calculations should only be viewed as a rough estimate. Nevertheless, it is clear that, despite the small size of FIS, the tyrosine environments play important roles in its fluorescence properties. While the tyrosines were observed to contribute different amounts to the WT fluorescence, Tyr51 appears to be a key residue for modulating the local environments in FIS, as its mutation severely affected the observed fluorescence and near-UV CD signals. We believe that the Y51F mutation affects the signals by altering the interactions within the C-terminal hydrogen-bonding network.

Even though tryptophan fluorescence has dominated as the probe of choice for monitoring protein folding (*88*), this study shows that tyrosine residues can serve as good fluorescence probes and emphasizes their usefulness to study the importance of hydrogen bonding via the conservative Tyr to Phe mutations.

ACKNOWLEDGMENT

We thank Dr. Dmitri Zagorevski for mass spectrometry analyses and the Department of Chemistry and Chemical Biology for support of the mass spectrometry facility. The electrospray ionization and MALDI-TOF mass spectrometers were obtained through NSF Grants CHE-0078056 and CHE-0091892.

REFERENCES

1. Stickle, D. F., Presta, L. G., Dill, K. A., and Rose, G. D. (1992) Hydrogen bonding in globular proteins, *J. Mol. Biol. 226*, 1143−1159.
2. Rose, G. D., and Wolfenden, R. (1993) Hydrogen bonding, hydrophobicity, packing, and protein folding, *Annu. Rev. Biophys. Biomol. Struct. 22*, 381−415.
3. Myers, J. K., and Pace, C. N. (1996) Hydrogen bonding stabilizes globular proteins, *Biophys. J. 71*, 2033−2039.
4. Jaenicke, R. (2000) Stability and stabilization of globular proteins in solution, *J. Biotechnol. 79*, 193−203.

5. Pace, C. N. (2001) Polar group burial contributes more to protein stability than nonpolar group burial, *Biochemistry 40*, 310−313.
6. Takano, K., Yamagata, Y., and Yutani, K. (2001) Contribution of polar groups in the interior of a protein to the conformational stability, *Biochemistry 40*, 4853−4858.
7. Byrne, M. P., Manuel, R. L., Lowe, L. G., and Stites, W. E. (1995) Energetic contribution of side chain hydrogen bonding to the stability of staphylococcal nuclease, *Biochemistry 34*, 13949−13960.
8. Yamagata, Y., Kubota, M., Sumikawa, Y., Funahashi, J., Takano, K., Fujii, S., and Yutani, K. (1998) Contribution of hydrogen bonds to the conformational stability of human lysozyme: calorimetry and X-ray analysis of six tyrosine → phenylalanine mutants, *Biochemistry 37*, 9355−9362.
9. Kim, D. H., Jang, D. S., Nam, G. H., Choi, G., Kim, J. S., Ha, N. C., Kim, M. S., Oh, B. H., and Choi, K. Y. (2000) Contribution of the hydrogen-bond network involving a tyrosine triad in the active site to the structure and function of a highly proficient ketosteroid isomerase from *Pseudomonas putida* biotype B, *Biochemistry 39*, 4581−4589.
10. Pace, C. N., Horn, G., Hebert, E. J., Bechert, J., Shaw, K., Urbanikova, L., Scholtz, J. M., and Sevcik, J. (2001) Tyrosine hydrogen bonds make a large contribution to protein stability, *J. Mol. Biol. 312*, 393−404.
11. Kuliopulos, A., Mildvan, A. S., Shortle, D., and Talalay, P. (1989) Kinetic and ultraviolet spectroscopic studies of active-site mutants of delta 5−3-ketosteroid isomerase, *Biochemistry 28*, 149−159.
12. Entsch, B., Palfey, B. A., Ballou, D. P., and Massey, V. (1991) Catalytic function of tyrosine residues in para-hydroxybenzoate hydroxylase as determined by the study of site-directed mutants, *J. Biol. Chem. 266*, 17341−17349.
13. Lee, M. E., Dyer, D. H., Klein, O. D., Bolduc, J. M., Stoddard, B. L., and Koshland, D. E., Jr. (1995) Mutational analysis of the catalytic residues lysine 230 and tyrosine 160 in the NADP(+)-dependent isocitrate dehydrogenase from *Escherichia coli*, *Biochemistry 34*, 378−384.
14. Yagi, H., Tozawa, K., Sekino, N., Iwabuchi, T., Yoshida, M., and Akutsu, H. (1999) Functional conformation changes in the TF-(1)-ATPase beta subunit probed by 12 tyrosine residues, *Biophys. J. 77*, 2175−2183.
15. Yudt, M. R., Vorojeikina, D., Zhong, L., Skafar, D. F., Sasson, S., Gasiewicz, T. A., and Notides, A. C. (1999) Function of estrogen receptor tyrosine 537 in hormone binding, DNA binding, and transactivation, *Biochemistry 38*, 14146−14156.
16. Mailfait, S., Belaiche, D., Kouach, M., Dallery, N., Chavatte, P., Formstecher, P., and Sablonniere, B. (2000) Critical role of tyrosine 277 in the ligand-binding and transactivating properties of retinoic acid receptor alpha, *Biochemistry 39*, 2183−2192.
17. Toth-Zsamboki, E., Oury, C., Watanabe, H., Nilius, B., Vermylen, J., and Hoylaerts, M. F. (2002) The intracellular tyrosine residues of the ATP-gated P2X1 ion channel are essential for its function, *FEBS Lett. 524*, 15−19.
18. Stenberg, G., Abdalla, A. M., and Mannervik, B. (2000) Tyrosine 50 at the subunit interface of dimeric human glutathione transferase P1-1 is a structural key residue for modulating protein stability and catalytic function, *Biochem. Biophys. Res. Commun. 271*, 59−63.
19. Baker, C. H., Tomlinson, S. R., Garcia, A. E., and Harman, J. G. (2001) Amino acid substitution at position 99 affects the rate of CRP subunit exchange, *Biochemistry 40*, 12329−12338.
20. Kim, D., and Park, C. (1993) Fluorescence properties of the three tyrosine residues in the ribose-binding protein, *Biochem. Biophys. Res. Commun. 195*, 1237−1244.
21. Li, Y. K., Kuliopulos, A., Mildvan, A. S., and Talalay, P. (1993) Environments and mechanistic roles of the tyrosine residues of Δ^5-3-ketosteroid isomerase, *Biochemistry 32*, 1816−1824.
22. Wu, P., Li, Y. K., Talalay, P., and Brand, L. (1994) Characterization of the three tyrosine residues of Δ^5-3-ketosteroid isomerase by time-resolved fluorescence and circular dichroism, *Biochemistry 33*, 7415−7422.
23. Thompson, T. M., Mark, B. L., Gray, C. W., Terwilliger, T. C., Sreerama, N., Woody, R. W., and Gray, D. M. (1998) Circular dichroism and electron microscopy of a core Y61F mutant of the F1 gene 5 single-stranded DNA-binding protein and theoretical analysis of CD spectra of four Tyr → Phe substitutions, *Biochemistry 37*, 7463−7477.
24. Sreerama, N., Manning, M. C., Powers, M. E., Zhang, J. X., Goldenberg, D. P., and Woody, R. W. (1999) Tyrosine, phenylalanine, and disulfide contributions to the circular dichroism of proteins: circular dichroism spectra of wild-type and mutant bovine pancreatic trypsin inhibitor, *Biochemistry 38*, 10814−10822.
25. Jeong, J. K., Shin, H. J., Kim, J. W., Lee, C. H., Kim, H. D., and Lim, W. K. (2003) Fluorescence and folding properties of Tyr mutant tryptophan synthase alpha-subunits from *Escherichia coli*, *Biochem. Biophys. Res. Commun. 300*, 29−35.
26. Daubner, S. C., and Fitzpatrick, P. F. (1998) Mutation to phenylalanine of tyrosine 371 in tyrosine hydroxylase increases the affinity for phenylalanine, *Biochemistry 37*, 16440−16444.
27. Waldman, A. D., Clarke, A. R., Wigley, D. B., Hart, K. W., Chia, W. N., Barstow, D., Atkinson, T., Munro, I., and Holbrook, J. J. (1987) The use of site-directed mutagenesis and time-resolved fluorescence spectroscopy to assign the fluorescence contributions of individual tryptophan residues in *Bacillus stearothermophilus* lactate dehydrogenase, *Biochim. Biophys. Acta 913*, 66−71.
28. Loewenthal, R., Sancho, J., and Fersht, A. R. (1991) Fluorescence spectrum of barnase: contributions of three tryptophan residues and a histidine-related pH dependence, *Biochemistry 30*, 6775−6779.
29. Smith, C. J., Clarke, A. R., Chia, W. N., Irons, L. I., Atkinson, T., and Holbrook, J. J. (1991) Detection and characterization of intermediates in the folding of large proteins by the use of genetically inserted tryptophan probes, *Biochemistry 30*, 1028−1036.
30. Mann, C. J., Royer, C. A., and Matthews, C. R. (1993) Tryptophan replacements in the trp aporepressor from *Escherichia coli*: probing the equilibrium and kinetic folding models, *Protein Sci. 2*, 1853−1861.
31. Hasselbacher, C. A., Rusinova, E., Waxman, E., Rusinova, R., Kohanski, R. A., Lam, W., Guha, A., Du, J., Lin, T. C., Polikarpov, I., et al. (1995) Environments of the four tryptophans in the extracellular domain of human tissue factor: comparison of results from absorption and fluorescence difference spectra of tryptophan replacement mutants with the crystal structure of the wild-type protein, *Biophys. J. 69*, 20−29.
32. Szpikowska, B. K., and Mas, M. T. (1996) Urea-induced equilibrium unfolding of single tryptophan mutants of yeast phosphoglycerate kinase: evidence for a stable intermediate, *Arch. Biochem. Biophys. 335*, 173−182.
33. Callis, P. R. (1997) 1La and 1Lb transitions of tryptophan: applications of theory and experimental observations to fluorescence of proteins, *Methods Enzymol. 278*, 113−150.
34. de Antonio, C., Martinez del Pozo, A., Mancheno, J. M., Onaderra, M., Lacadena, J., Martinez-Ruiz, A., Perez-Canadillas, J. M., Bruix, M., and Gavilanes, J. G. (2000) Assignment of the contribution of the tryptophan residues to the spectroscopic and functional properties of the ribotoxin alpha-sarcin, *Proteins 41*, 350−361.
35. Doyle, T. C., Hansen, J. E., and Reisler, E. (2001) Tryptophan fluorescence of yeast actin resolved via conserved mutations, *Biophys. J. 80*, 427−434.
36. Finkel, S. E., and Johnson, R. C. (1992) The Fis Protein: it's not just for DNA inversion anymore, *Mol. Microbiol. 6*, 3257−3265.
37. Osuna, R., Lienau, D., Hughes, K. T., and Johnson, R. C. (1995) Sequence, regulation, and functions of fis in *Salmonella typhimurium*, *J. Bacteriol. 177*, 2021−2032.
38. Beach, M. B., and Osuna, R. (1998) Identification and characterization of the fis operon in enteric bacteria, *J. Bacteriol. 180*, 5932−5946.
39. Johnson, R. C., Bruist, M. F., and Simon, M. I. (1986) Host protein requirements for in vitro site-specific DNA inversion, *Cell 46*, 531−539.
40. Koch, C., and Kahmann, R. (1986) Purification and properties of the *Escherichia coli* host factor required for inversion of the G segment in bacteriophage Mu, *J. Biol. Chem. 261*, 15673−15678.
41. Haffter, P., and Bickle, T. A. (1987) Purification and DNA-binding properties of FIS and Cin, two proteins required for the bacteriophage P1 site-specific recombination system, cin, *J. Mol. Biol. 198*, 579−587.
42. Kostrewa, D., Granzin, J., Koch, C., Choe, H. W., Raghunathan, S., Wolf, W., Labahn, J., Kahmann, R., and Saenger, W. (1991) Three-dimensional structure of the *E. coli* DNA-binding protein FIS, *Nature 349*, 178−180.
43. Cheng, Y. S., Yang, W. Z., Johnson, R. C., and Yuan, H. S. (2000) Structural analysis of the transcriptional activation on Fis: crystal structures of six Fis mutants with different activation properties, *J. Mol. Biol. 302*, 1139−1151.

44. Hobart, S. A., Meinhold, D. W., Osuna, R., and Colon, W. (2002) From two-state to three-state: Effect of P61A mutation on the dynamics and stability of the factor for inversion stimulation results in an altered equilibrium denaturation mechanism, *Biochemistry 41*, 13744−13754.
45. Sambrook, J., Fritsch, E. F., and Maniatis, T. (1989) *Molecular Cloning: a laboratory manual*, 2nd ed., Cold Spring Harbor Laboratory, Cold Spring Harbor, NY.
46. Hobart, S. A., Ilin, S., Moriarty, D. F., Osuna, R., and Colon, W. (2002) Equilibrium denaturation studies of the E. coli factor for inversion stimulation: implications for in vivo function, *Protein Sci. 11*, 1671−1680.
47. Yuan, H. S., Finkel, S. E., Feng, J. A., Kaczor-Grzeskowiak, M., Johnson, R. C., and Dickerson, R. E. (1991) The molecular structure of wild-type and a mutant Fis protein: relationship between mutational changes and recombinational enhancer function or DNA binding, *Proc. Natl. Acad. Sci. U.S.A. 88*, 9558−9562.
48. Kostrewa, D., Granzin, J., Stock, D., Choe, H. W., Labahn, J., and Saenger, W. (1992) Crystal structure of the factor for inversion stimulation FIS at 2.0 A resolution, *J. Mol. Biol. 226*, 209−226.
49. Safo, M. K., Yang, W. Z., Corselli, L., Cramton, S. E., Yuan, H. S., and Johnson, R. C. (1997) The transactivation region of the fis protein that controls site-specific DNA inversion contains extended mobile beta-hairpin arms, *EMBO J. 16*, 6860−6873.
50. Eisenhaber, F., and Argos, P. (1993) Improved strategy in analytic surface calculation for molecular systems: handling of singularities and computational efficiency, *J. Comput. Chem. 14*, 1272−1280.
51. Eisenhaber, F., Lijnzaad, P., Argos, P., Sander, C., and Scharf, M. (1995) The double cubic lattice method: efficient approaches to numerical integration of surface area and volume and to dot surface contouring of molecular assemblies, *J. Comput. Chem. 16*, 273−284.
52. Altschul, S. F., Madden, T. L., Schaffer, A. A., Zhang, J., Zhang, Z., Miller, W., and Lipman, D. J. (1997) Gapped BLAST and PSI-BLAST: a new generation of protein database search programs, *Nucleic Acids Res. 25*, 3389−3402.
53. Corpet, F. (1988) Multiple sequence alignment with hierarchical clustering, *Nucleic Acids Res. 16*, 10881−10890.
54. Pace, C. N., Vajdos, F., Fee, L., Grimsley, G., and Theronica, G. (1995) How to measure and predict the molar absorption coefficient of a protein, *Protein Sci. 4*, 2411−2423.
55. Pace, C. N., Shirley, B. A., and Thomson, J. A. (1990) Measuring the conformational stability of a protein, in *Protein Structure: A Practical Approach* (Creighton, T. E., Ed.) pp 311−330, Oxford University Press, Oxford.
56. Johnson, R. C., and Simon, M. I. (1985) Hin-mediated site-specific recombination requires two 26 bp recombination sites and a 60 bp recombinational enhancer, *Cell 41*, 781−791.
57. Eftink, M. R. (1994) The use of fluorescence methods to monitor unfolding transitions in proteins, *Biophys. J. 66*, 482−501.
58. Bothner, B., Dong, X. F., Bibbs, L., Johnson, J. E., and Siuzdak, G. (1998) Evidence of viral capsid dynamics using limited proteolysis and mass spectrometry, *J. Biol. Chem. 273*, 673−676.
59. Schellman, J. A. (1978) Solvent denaturation, *Biopolymers 17*, 1305−1322.
60. Schellman, J. A. (1987) The thermodynamic stability of proteins, *Annu. Rev. Biophys. Biophys. Chem. 16*, 115−137.
61. Serrano, L., and Fersht, A. R. (1989) Capping and alpha-helix stability, *Nature 342*, 296−299.
62. Kellis, J. T., Jr., Nyberg, K., and Fersht, A. R. (1989) Energetics of complementary side-chain packing in a protein hydrophobic core, *Biochemistry 28*, 4914−4922.
63. Osuna, R., Finkel, S. E., and Johnson, R. C. (1991) Identification of two functional regions in Fis: the N-terminus is required to promote Hin-mediated DNA inversion but not lambda excision, *EMBO J. 10*, 1593−1603.
64. Serrano, L., Kellis, J. T., Jr., Cann, P., Andreas, M., and Fersht, A. R. (1992) The folding of an enzyme II. Substructure of barnase and the contribution of different interactions to protein stability, *J. Mol. Biol. 224*, 783−804.
65. Pace, C. N. (1995) Evaluating contribution of hydrogen bonding and hydrophobic bonding to protein folding, *Methods Enzymol. 259*, 538−554.
66. Fersht, A. R., Matouschek, A., and Serrano, L. (1992) The folding of an enzyme. I. Theory of protein engineering analysis of stability and pathway of protein folding, *J. Mol. Biol. 224*, 771−782.
67. Pace, C. N., Shirley, B. A., McNutt, M., and Gajiwala, K. (1996) Forces contributing to the conformational stability of proteins, *FASEB J. 10*, 75−83.
68. Fontana, A., Polverino de Laureto, P., De Filippis, V., Scaramella, E., and Zambonin, M. (1997) Probing the partly folded states of proteins by limited proteolysis, *Folding Des. 2*, R17−R26.
69. Hubbard, S. J. (1998) The structural aspects of limited proteolysis of native proteins, *Biochim. Biophys. Acta 1382*, 191−206.
70. Yuan, H. S., Wang, S. S., Yang, W.-Z., Finkel, S. E., and Johnson, R. C. (1994) The structure of Fis mutant $Pro^{61}Ala$ illustrates that the kink within the long α-helix is not due to the presence of the proline residue, *J. Biol. Chem. 269*, 28947−28954.
71. Jin, L., Fukayama, J. W., Pelczer, I., and Carey, J. (1999) Long-range effects on dynamics in a temperature-sensitive mutant of trp repressor, *J. Mol. Biol. 285*, 361−378.
72. Burley, S. K., and Petsko, G. A. (1985) Aromatic−aromatic interaction: A mechanism of protein structure stabilization, *Science 229*, 23−28.
73. Serrano, L., Bycroft, M., and Fersht, A. R. (1991) Aromatic−aromatic interactions and protein stability. Investigation by double-mutant cycles, *J. Mol. Biol. 218*, 465−475.
74. Pace, C. N., and Scholtz, J. M. (1998) A helix propensity scale based on experimental studies of peptides and proteins, *Biophys. J. 75*, 422−427.
75. Sekharudu, C., Ramakrishnan, B., Huang, B., Jiang, R. T., Dupureur, C. M., Tsai, M. D., and Sundaralingam, M. (1992) Crystal structure of the Y52F/Y73F double mutant of phospholipase A2: increased hydrophobic interactions of the phenyl groups compensate for the disrupted hydrogen bonds of the tyrosines, *Protein Sci. 1*, 1585−1594.
76. Machius, M., Declerck, N., Huber, R., and Wiegand, G. (2003) Kinetic stabilization of *Bacillus licheniformis* alpha-amylase through introduction of hydrophobic residues at the surface, *J. Biol. Chem. 278*, 11546−11553.
77. Shortle, D., and Meeker, A. K. (1986) Mutant forms of Staphylococcal nuclease with altered patterns of guanidine hydrochloride and urea denaturation, *Proteins 1*, 81−89.
78. Ball, C. A., Osuna, R., Ferguson, K. C., and Johnson, R. C. (1992) Dramatic changes in Fis levels upon nutrient upshift in *Escherichia coli*, *J. Bacteriol. 174*, 8043−8056.
79. Strickland, E. H. (1974) Aromatic contributions to circular dichroism spectra of proteins, *CRC Crit. Rev. Biochem. 2*, 113.
80. Dolgikh, D. A., Gilmanshin, R. I., Brazhnikov, E. V., Bychkova, V. E., Semisotnov, G. V., Venyaminov, S. Y., and Ptitsyn, O. B. (1981) α-Lactalbumin: compact state with fluctuating tertiary structure?, *FEBS Lett. 136*, 311−315.
81. Ohgushi, M., and Wada, A. (1983) 'Molten-globule state': a compact form of globular proteins with mobile side-chains, *FEBS Lett. 164*, 21−24.
82. Adler, A. J., Greenfield, N. J., and Fasman, G. D. (1973) Circular dichroism and optical rotatory dispersion of proteins and polypeptides, *Methods Enzymol. 27*, 675−735.
83. Brun, F., Toulme, J. J., and Helene, C. (1975) Interactions of aromatic residues of proteins with nucleic acids. Fluorescence studies of the binding of oligopeptides containing tryptophan and tyrosine residues to polynucleotides, *Biochemistry 14*, 558−563.
84. Mayer, R., Toulme, F., Montenay-Garestier, T., and Helene, C. (1979) The role of tyrosine in the association of proteins and nucleic acids. Specific recognition of single-stranded nucleic acids by tyrosine-containing peptides, *J. Biol. Chem. 254*, 75−82.
85. Ross, J. B., Laws, W. R., Rousslang, K. W., and Wyssbrod, H. R. (1992) Tyrosine fluorescence and phosphorescence from proteins and polypeptides, in *Topics in Fluorescence Spectroscopy* (Lackowicz, J. R., Ed.) Plenum Press, New York.
86. Marqusee, S., and Sauer, R. T. (1994) Contributions of a hydrogen bond/salt bridge network to the stability of secondary and tertiary structure in lambda repressor, *Protein Sci. 3*, 2217−2225.
87. Honig, B., and Yang, A. S. (1995) Free energy balance in protein folding, *Adv. Protein Chem. 46*, 27−58.
88. Lakowicz, J. R. (1999) *Principles of Fluorescence Spectroscopy*, 2nd ed., Kluwer Academic/Plenum Publishers, New York.
89. Kraulis, P. J. (1991) MOLSCRIPT: a program to produce both detailed and schematic plots of protein structures, *J. Appl. Crystallogr. 24*, 946−950.

BI035441K